THE JOURNAL OF BIOLOGICAL CHEMISTRY Vol. 276, No. 14, Issue of April 6, pp. 11021–11030, 2001
Printed in U.S.A.

Ligand-induced Dynamic Membrane Changes and Cell Deletion Conferred by Vanilloid Receptor 1*

Received for publication, September 13, 2000, and in revised form, December 11, 2000
Published, JBC Papers in Press, December 21, 2000, DOI 10.1074/jbc.M008392200

Zoltan Olah‡§¶, Tamas Szabo§‖, Laszlo Karai‡§, Chris Hough, R. Douglas Fields‡‡, Robert M. Caudle‡, Peter M. Blumberg‖, and Michael J. Iadarola‡**

*From the ‡Neuronal Gene Expression Unit, Pain and Neurosensory Mechanisms Branch, NIDCR, the ‖Laboratory of Cellular Carcinogenesis and Tumor Promotion, NCI, the **Neuronal Excitability Section, Epilepsy Branch, NINDS, and the ‡‡Laboratory of Developmental Neurobiology, NICHD, National Institutes of Health, Bethesda, Maryland 20892*

The real time dynamics of vanilloid-induced cytotoxicity and the specific deletion of nociceptive neurons expressing the wild-type vanilloid receptor (VR1) were investigated. VR1 was C-terminally tagged with either the 27-kDa enhanced green fluorescent protein (eGFP) or a 12-amino acid ϵ-epitope. Upon exposure to resiniferatoxin, VR1eGFP- or VR1ϵ-expressing cells exhibited pharmacological responses similar to those of cells expressing the untagged VR1. Within seconds of vanilloid exposure, the intracellular free calcium ($[Ca^{2+}]_i$) was elevated in cells expressing VR1. A functional pool of VR1 also was localized to the endoplasmic reticulum that, in the absence of extracellular calcium, also was capable of releasing calcium upon agonist treatment. Confocal imaging disclosed that resiniferatoxin treatment induced vesiculation of the mitochondria and the endoplasmic reticulum (~1 min), nuclear membrane disruption (5–10 min), and cell lysis (1–2 h). Nociceptive primary sensory neurons endogenously express VR1, and resiniferatoxin treatment induced a sudden increase in $[Ca^{2+}]_i$ and mitochondrial disruption which was cell-selective, as glia and non-VR1-expressing neurons were unaffected. Early hallmarks of cytotoxicity were followed by specific deletion of VR1-expressing cells. These data demonstrate that vanilloids disrupt vital organelles within the cell body and, if administered to sensory ganglia, may be employed to rapidly and selectively delete nociceptive neurons.

Capsaicin (CAP),[1] a well characterized membrane-permeable vanilloid agonist, has potent stimulatory actions on nociceptive neurons and causes loss of unmyelinated "C"-type sensory afferents when administered to newborn animals (1, 2). Similarly, resiniferatoxin (RTX), an ultrapotent capsaicin analogue, can deplete [^{3}H]RTX-binding sites from the brain stem, the sensory ganglia (dorsal root and trigeminal), and the spinal cord with a mechanism that has not been fully elucidated (3, 4). Both systemic and epidural administration of RTX to adult rats produce analgesia to subsequent noxious thermal stimulation (5). Depending on concentration, duration of exposure, and route of administration, vanilloid ligands may either desensitize the nociceptive primary afferent nerve ending or completely delete the neuron itself (6–8). Previous studies investigating the processes of desensitization and cell loss mainly examined whole animals or primary cultures of dorsal root ganglia, where nociceptive neuronal cell bodies are located. The cloning of the first isotype of the vanilloid receptor (VR1) provides a means to investigate more fully the molecular and cell biological mechanisms of pain signal transduction and the processes underlying susceptibility of VR1-expressing cells to impairment upon exposure to vanilloid agonists (9). The VR1 has been characterized as a Ca^{2+} ionophore (9, 10); thus, it also provides a very specific molecule with which to investigate the role of ligand-activated transmembrane calcium fluxes in cellular toxicity.

The VR1 exhibits homology to Ca^{2+} store-dependent TRP channels. In contrast to TRPs, which regulate intracellular calcium stores, VR1 confers two pivotal sensory functions. VR1 transduces chemical (vanilloids and pH) and physical (heat) stimuli at the molecular level, generating action potentials in nociceptive nerve endings, and ultimately leading to sensations of heat, thermal pain, and inflammatory pain (10, 11). Loss of moderately noxious heat and vanilloid-stimulated sensory functions has been verified in animals lacking VR1 (11, 12). VR1 mRNA is expressed with remarkable cell and tissue specificity in the DRG. Immunocytochemistry demonstrates VR1 throughout the peripheral endings, cell body, and presynaptic terminals of small size dorsal root ganglion (DRG) neurons (10, 13). These sites coincide well with regional localization of [^{3}H]RTX binding (3, 4). The ability of CAP and RTX to displace [^{3}H]RTX binding in the spinal cord and DRG as well as similarities in [^{3}H]RTX binding studies with recombinantly expressed VR1 suggest that both vanilloids act on the same receptors (14).

Previous studies with vanilloids have shown that vanilloid administration can lead to cell type-specific membrane damage. Long term exposure to vanilloids causes profound ultrastructural changes in DRG neurons (15, 16). VR1-specific antibodies have been used in intracellular localization by light and electron microscopy, but the functional relationship of these morphological observations to the observed cell damage has not been explored (10, 13). Immunostaining of fixed cells often limits detailed visual observation of rapid intracellular processes. In the present paper, we used fluorescence confocal microscopy and real time imaging of enhanced green fluores-

* The costs of publication of this article were defrayed in part by the payment of page charges. This article must therefore be hereby marked "*advertisement*" in accordance with 18 U.S.C. Section 1734 solely to indicate this fact.

§ These authors contributed equally to this work.

¶ To whom correspondence should be addressed: Bldg. 49, Rm. 1A19, NIH, 49 Convent Dr., MSC-4410, Bethesda, MD 20892-4410. Tel.: 301-496-2755; Fax: 301-402-0667; E-mail: zoltan.olah@nih.gov.

[1] The abbreviations used are: CAP, capsaicin; CPZ, capsazepine; OLV, olvanil; RTX, resiniferatoxin; VR1, vanilloid receptor; TRP, Ca^{2+} store-dependent channel; DRG, dorsal root ganglion; eGFP, enhanced green fluorescent protein; VR1eGFP, C-terminally eGFP-tagged vanilloid receptor; VR1ϵ, C-terminally ϵ-tagged vanilloid receptor; ER, endoplasmic reticulum; $[Ca^{2+}]_i$, intracellular free calcium; NGF, neuronal growth factor; FUDR, 5-fluoro-2′-deoxyuridine; DMEM, Dulbecco's modified Eagle's medium; RT-PCR, reverse transcriptase-polymerase chain reaction; PI, propidium iodide; MTH, metallothionein.

cent protein (eGFP)-tagged VR1 (VR1eGFP) to examine simultaneously both the morphological and functional molecular processes underlying the immediate effects of vanilloid exposure on the perikarya of cells and neurons with high temporal and spatial resolution. Biochemical functions in the plasma membrane (membrane potential changes, calcium uptake, and [^{3}H]RTX binding) similar to wild-type VR1 were readily observed with the chimeric VR1eGFP. In addition, another active pool of VR1 was located at the endoplasmic reticulum (ER), which also reacted within seconds to vanilloid treatment.

Exposure of VR1-expressing cells to vanilloids produced a rapidly evolving cytotoxicity. This commenced with a rise in $[Ca^{2+}]_i$, which quickly surpassed the Ca^{2+} tolerance or sequestration capacity of the mitochondria. Subsequently, nuclear envelope shrinkage and blebbing occurred, followed by cell death. The effect of elevated $[Ca^{2+}]_i$ on vital organelles suggests that targeted administration of vanilloid agents to the cell body can rapidly compromise and then eliminate (within hours) VR1-expressing nociceptive neurons. In fact, immunoblot analysis of protein extracts from primary DRG cultures showed that treatment with any of several vanilloid agonists eliminated cells expressing the VR1.

EXPERIMENTAL PROCEDURES

RT-PCR Cloning and Epitope Tagging—To obtain VR1-specific mRNA, 100 DRGs were rapidly removed from 12 adult Harlan Sprague-Dawley rats. Total RNA was isolated with the TRI REAGENT (Molecular Research Center Inc., Cincinnati, OH). A fragment, comprising the sequence between the *Xba*I and *Afl*III sites of rat VR1, was amplified first by the Access RT-PCR system (Promega) and then cloned into the BlueScript vector (Stratagene). The missing 5′-sequence was added likewise with the *Sac*I and *Xba*I sites. At the 5′ ends of the N- and C-terminal fragments, the *Sac*I and *Afl*III sites (underlined) were incorporated with forward primers AGATCTCGAGCTCAAATGGAACA-ACGGGCTAGCTTAGACTC and CTGTATTCCACATGTCTGGAGCTG-TTCAAGTTC, respectively. As reverse primers ACTGAGTCCCGGGC-GCTGATGTCTGCAGGCT and CACACAGTCGACTTTCTCCCCTGG-GACCATGGAATCCTT were used, in which the *Xba*I and *Sal*I sites were incorporated, respectively. The *Sac*I-*Afl*III and the RT-PCR-generated *Afl*III-*Sal*I fragments were triple-ligated into a *Sac*I and *Sal*I cut pEGFP-N3 vector (CLONTECH). The immediate early promoter of the cytomegalovirus in the pEGFP-N3 vector was employed to produce the full-length VR1 with the eGFP tag. Rat VR1 with the short, 12-amino acid ϵ-tag (KGFSYFGEDLMP) was constructed in a vector, pϵMTH, driven by the metallothionein promoter (17). Briefly, *Sal*I and *Mlu*I restriction endonuclease sites were incorporated into the VR1 PCR fragment amplified using the forward AGTAGTGTCGACGAACA-ACGGGCTAGCTTAGACTCA and reverse TTGTTGACGCGTTTTCTC-CCCTGGGACCATGGAATC primers, respectively. After cutting the PCR fragment with these enzymes the size-separated cDNA insert was ligated in pϵMTH at the compatible *Xho*I and *Mlu*I sites (17). The chimeric constructs were verified by sequencing and transiently transfected in COS7, HEK293, and NIH 3T3 cells employing the protocol provided for the LipofectAMINE reagent (Life Technologies, Inc.). The basal activity of the pϵMTH promoter was used in NIH 3T3 cells to produce VR1ϵ, yet prevent toxicity from long term, high level expression.

Electrophysiology—For patch clamp studies, VR1eGFP-expressing COS7 and HEK293 cells were voltage-clamped in Krebs buffer containing (in mM) NaCl (124), KCl (4.9), KH_2PO_4 (1.2), $MgSO_4$ (2.4), $CaCl_2$ (2.5), $NaHCO_3$ (25.6), and glucose (10), using an Axopatch 200B amplifier (Axon Instruments, Foster City, CA). Recordings were carried out with patch electrodes (2–10 MΩ) filled with 10 mM HEPES buffer (pH 7.4) containing (in mM) CsCl (120), tetraethylammonium chloride (20), $CaCl_2$ (1), $MgCl_2$ (2), EGTA (10), ATP (4), and GTP (0.5).

Determination of Ca^{2+} Uptake—Cells were transfected at 80% confluence in 75-cm^2 T-flasks with 20 μg of VR1eGFP or VR1ϵ plasmids. After 48 h, 5×10^4 cells were detached from the plastic surface by serum-free DMEM containing 1 mM EDTA and then washed two times and resuspended in medium without EDTA. Cell suspensions were incubated in serum-free DMEM containing 1 μCi/ml $^{45}Ca^{2+}$ and ligands as indicated for 15 min at 35 °C in 96-well filtration plates (MultiScreen-DV, Millipore, Marlborough, MA). Ca^{2+} uptake was terminated on ice, and samples were processed and analyzed as described (18).

[^{3}H]RTX Binding—48 h after transfection in 75-cm^2 T-flasks, cells were detached from the plastic surface by serum-free DMEM containing 1 mM EDTA and then washed and resuspended in 10 mM HEPES (pH 7.4) buffer, containing (in mM) KCl (5), NaCl (5.8), $MgCl_2$ (2), $CaCl_2$ (0.75), glucose (12), and sucrose (137). Intact cells were incubated (10^5/well) in a filtration plate with 200 pM [^{3}H]RTX for 60 min at 37 °C and then processed as described earlier (5). Data were analyzed by computer fit to the Hill equation as noted previously (18, 19).

Fluorescent Confocal Microscopy—COS7, NIH 3T3, and HEK293 cells were seeded on 25-mm coverslips and transfected with 1 μg each of the plasmid constructs, cultured for 24 h post-transfection at 35 °C, then mounted in a 1-ml chamber and examined with a MRC-1024 Bio-Rad confocal microscope. To study the two- and three-dimensional distribution of fluorescent chimeric proteins, each *x-y* plane was scanned over 1 s and at 0.2-μm increments in the *z* axis mode. To label different subcellular compartments of live cells fluorescently, the ER marker eGFP-KDEL (CLONTECH) was transiently transfected in COS7 and NIH 3T3 cells. To label mitochondria, MitoTracker (Molecular Probes) dye was incubated for 30 min at a 250 nM concentration; the cells were then washed with Hanks' balanced salt solution supplemented with 1 mM $CaCl_2$ and 0.8 mM $MgCl_2$, buffered with 15 mM HEPES (pH 7.4) (HBSSH).

$[Ca^{2+}]_i$ Microfluorometry—For determination of $[Ca^{2+}]_i$, cells were cultured in glass bottom dishes (MatTek Corp., Ashland, MA) and then transfected with 2 μg of VR1eGFP plasmid. After 24 h in culture, cells were loaded with Fura 2/AM (Molecular Probes, Eugene, OR) for 30 min at 37 °C. Single cells expressing the VR1eGFP construct were identified by eGFP fluorescence and were selected based on visual inspection of fluorescence intensity. In all experiments, cells exhibiting intermediate fluorescence in comparison to other cells in the same dish were picked for analysis. To determine the $[Ca^{2+}]_i$, the excitation ratio of Fura-2 at 340 and 380 nm was recorded photometrically in Krebs' buffer at a 10-Hz sampling rate and integrated over 0.5 s, as described previously (20). $[Ca^{2+}]_i$ was calculated using the ratio based equation (21).

Ratiometric Imaging of $[Ca^{2+}]_i$ Employing Confocal Microscopy—Cells cultured on poly-D-lysine-coated coverslips were pre-loaded with 5 μM Indo-1 AM dye. After incubation for 30 min at 34 °C, the cells were washed three times in HBSSH to remove excess dye and examined under the confocal microscope. To record in "zero" extracellular Ca^{2+} cells were washed four times (5 min each) in HBSSH containing no $CaCl_2$ and 1 mM EGTA and imaged in the same medium. Groups of cells expressing VR1eGFP or small size neurons were selected under the microscope. To quantitate the fluorescence ratio, perikarya of the cells were marked with the graphic tools of the LaserSharp software in the field of a × 40 objective of the Bio-Rad confocal system. Ratiometric imaging was performed at 10-s intervals with an UV laser, and the ratio of fluorescence intensity emitted at 405 and 485 was calculated.

DRG Culture—DRG neuron-enriched cultures were prepared from embryonic rats (E16). Briefly, embryos were removed from the uterus and placed in Petri dishes containing Lebowitz medium (Life Technologies, Inc.). The cords were dissected, and the DRGs were stripped off with the meninges. Cells were digested in 0.125% trypsin at 37 °C for 20 min. For plating, dissociated cells were changed into minimal essential medium containing 5% horse serum and 50 ng/ml nerve growth factor (NGF). Cells were seeded on 25-mm glass coverslips or on multiwell plates. Surfaces were coated with poly-D-lysine and laminin. DRG cultures were maintained in DMEM containing 20 mM HEPES, 7.5% fetal bovine serum, 7.5% horse serum, 5 mg/ml uridine supplemented with 2 mg/ml FUDR to inhibit cell division and 50 ng/ml NGF to promote neuronal survival and differentiation. Cultures were selected in this medium for 1 week, at which point well differentiated neurons and nondividing cells dominated the population. Primary DRG cultures in this stage were used in confocal microscopy.

Western Blotting—Total protein extracts were prepared in denaturing SDS buffer and analyzed for immunoreactivity by Western blotting similar to that described by us previously (17). VR1-specific antibody was raised in rabbits employing the N-terminal MEQRASLDSEES-ESPPQE peptide of rat VR1 conjugated to keyhole limpet hemocyanin as immunogen. Immune sera were affinity purified against the peptide used for immobilization. The specific antibody fraction eluted from the affinity column was diluted 1000-fold for further characterization in Western blot and immunocytochemistry experiments. This antibody fraction recognizes the native rat VR1, as illustrated in Fig. 11, and the chimeric VR1eGFP and VR1ϵ (data not shown). Stripping of nitrocellulose blotting filters (Bio-Rad) was carried out in 200 ml of 50 mM Tris-HCl buffer (pH 7.5) containing 2% SDS and 0.1 β-mercaptoethanol at 65 °C for 1 h. Stripped blots were reanalyzed for tagged fusion proteins either with the GFP (CLONTECH) or the ϵPKC-specific anti-

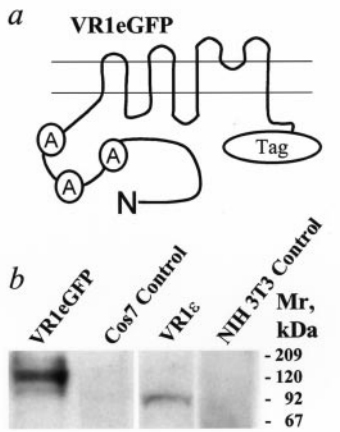

FIG. 1. *a*, schematic representation of C-terminally tagged VR1. *b,* Western blot analysis of the chimeric proteins. To generate VR1eGFP and VR1ϵ, the stop codon of the wild-type VR1 was deleted and the C-terminal domain extended with the cDNA coding for the enhanced green fluorescent protein or the ϵ-tag as described under "Experimental Procedures." The intracellular ankyrin repeats, the enhanced green fluorescent protein-, and ϵ-epitope-tagged chimera proteins are abbreviated as A, VR1eGFP, and VR1ϵ, respectively. *b,* VR1eGFP and VR1ϵ plasmids were transfected in HEK293 and NIH 3T3 cells, respectively. After 48 h 35 μg of total protein extract, prepared in SDS sample buffer, was analyzed for the eGFP (*lanes 1* and *2*) and ϵ-tag immunoreactivities (*lanes 3* and *4*) by Western blotting, employing eGFP and ϵ-tag specific antibodies, respectively. Enhanced chemiluminescence was employed to visualize the interaction with the primary antibodies, as described under "Experimental Procedures." The molecular weight was calculated from the mobility of the immunoreactive protein band compared with protein standards.

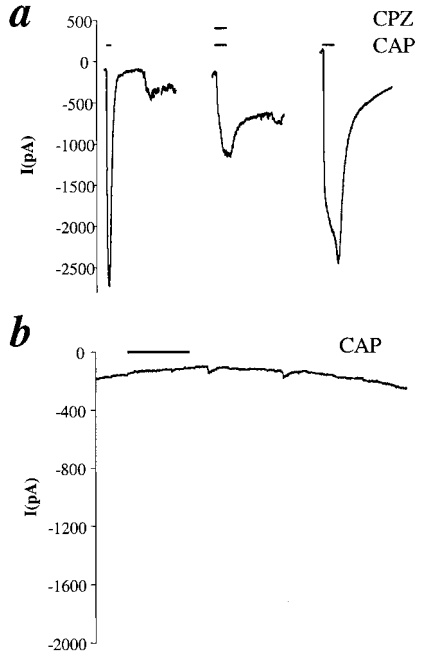

FIG. 2. **Vanilloid currents in transiently transfected HEK293 cells.** HEK293 cells were cultured on laminin-coated coverslips in 6-well plates and transfected with VR1eGFP (*a*) or eGFP plasmids (*b*). After 48 h, cells expressing the fluorescent proteins were selected for voltage clamp assays. The holding potential for all of the cells was −60 mV. *a,* 10 μM CAP was bath-perfused for 30 s for the first application and 1 min for subsequent applications to induce currents in VR1eGFP-expressing cells. The first treatment with CAP was shortened to reduce the amount of receptor desensitization. The antagonist 10 μM CPZ attenuated the capsaicin-induced current (n = 4 cells). The drugs were washed out of the bath for 10 min between applications. *b,* capsaicin (10 μM) (n = 4 cells) did not evoke currents in eGFP transfected HEK293 cells. Drug application was 1 min.

bodies (Life Technologies, Inc.), prepared in rabbits. To assess equal loading, filters were re-probed with a rat cytochrome *c*-specific monoclonal antibody (6H2.B4) as suggested by the manufacturer (Transduction Laboratories). Antibodies for Western blotting were used at a 1:1000 dilution. To visualize the interaction with the primary antibodies, enhanced chemiluminescence technology was employed according to the protocol provided by the manufacturer (New England Biolabs).

RESULTS

VR1ϵ and VR1eGFP plasmid constructs were expressed in COS7, HEK293, and NIH 3T3 cells by transient transfection. Western blot analysis with polyclonal eGFP and ϵ-tag-specific antibodies demonstrated that the VR1eGFP and VR1ϵ chimeric proteins expressed in HEK293 and NIH 3T3 cells were of the appropriate sizes, 120 and 93 kDa, respectively (Fig. 1, *1st* and *3rd lanes*). No tag-related immunoreactivity was found in the nontransfected host cells (Fig. 1, *2nd* and *4th lanes*). Repeated Western analyses with GFP- and ϵ-tag-specific antibodies showed no proteolytic cleavage of the VR1 chimeric proteins (data not shown). These transiently transfected plasmid constructs expressed proteins that exhibited identical molecular weights after the tag-specific antibodies were removed and the blots re-probed with the N-terminal specific VR1 antibody (data not shown).

To study the electrophysiological properties of C-terminally eGFP-tagged VR1, plasmid constructs producing VR1eGFP and eGFP as a control were transiently expressed in HEK293 cells. Green fluorescent cells of medium fluorescence intensity were voltage-clamped, and the holding potential was adjusted to −60 mV. Capsaicin (10 μM) induced a large inward current (Fig. 2*a*). Similar currents were also evoked by administration of 125 pM RTX to the cells; however, the currents rapidly desensitized to repeated applications (n = 6) (data not shown). Capsaicin was noted to be less effective at inducing desensitization than RTX; therefore, CAP was used in experiments that required repeated application of vanilloid ligands (*e.g.* Fig. 2). As expected for a functional recombinant, the VR1eGFP-mediated current was attenuated by coincubation of an antagonist, 10 μM capsazepine (CPZ). The current *versus* voltage relationship demonstrated that the VR1eGFP-mediated current was not particularly voltage-sensitive. The reversal potential was near 0 mV, suggesting mixed cation selectivity for the channel (data not shown). Cells transfected with eGFP did not demonstrate currents when exposed to either CAP or RTX (Fig. 2*b* and data not shown). Likewise, nontransfected HEK293 cells did not demonstrate RTX-evoked currents. Overall, the electrophysiological properties of the eGFP-tagged VR1 were very similar to those described for nontagged VR1 (9).

In accordance with the electrophysiological data, exposure to RTX induced Ca^{2+} uptake in VR1eGFP-expressing HEK293 and COS7 cells. This ligand-induced Ca^{2+} influx (Fig. 3*a*) further confirms the presence of VR1eGFP at the plasma membrane. RTX induced $^{45}Ca^{2+}$ uptake with an ED_{50} = 100 ± 50 pM (n = 3) whereas that for CAP was 0.5 ± 0.15 μM (data not shown). Similar results were obtained for VR1 tagged with the 12-amino acid ϵ-epitope in place of the eGFP tag. This indicates that a C-terminal tag, *per se*, does not significantly change Ca^{2+} uptake parameters. In addition, RTX-induced $^{45}Ca^{2+}$ uptake was completely blocked by 10 μM CPZ in VR1eGFP- (Fig. 3*a*) and VR1ϵ−expressing cells (not shown).

The curves in Fig. 3*b* demonstrate the quantitative characteristics of [^{3}H]RTX binding to eGFP-tagged and ϵ-tagged VR1 expressed in COS7 cells. Both tagged recombinants exhibited a high affinity, dose-dependent interaction (K_d ~ 150 ± 10 pM, n = 6) and cooperativity among the receptors (Hill coefficient = 1.5–2). [^{3}H]RTX binding was almost completely inhibited by coincubation of 10 μM CPZ. No significant [^{3}H]RTX binding was

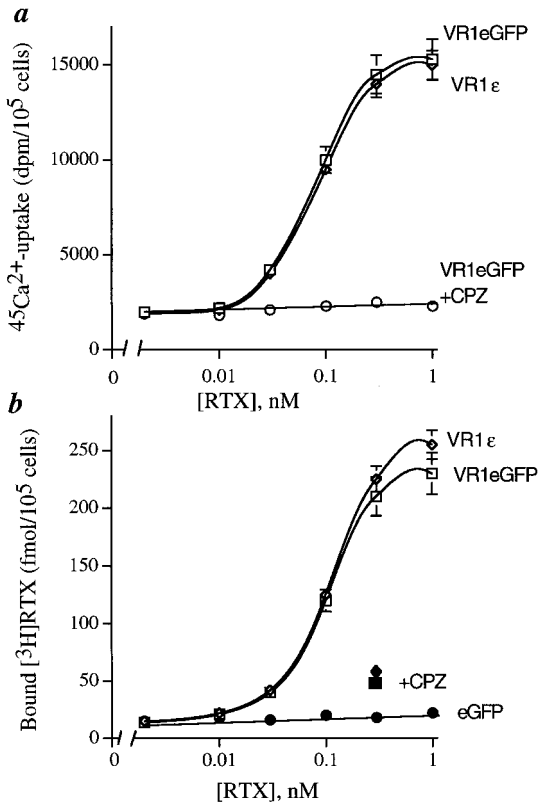

FIG. 3. *a*, RTX-induced Ca^{2+}-ionophore activity of the VR1eGFP (*squares*) and VR1ϵ (*diamonds*). HEK293 cells were transfected for 48 h with the plasmid constructs and then $^{45}Ca^{2+}$-uptake was induced with the indicated concentrations of RTX. The $^{45}Ca^{2+}$ uptake experiments were carried out as described under "Experimental Procedures." The results were analyzed by fitting the Hill equation to the data points. The effects of 10 μM CPZ cotreatment with increasing concentrations of RTX on $^{45}Ca^{2+}$ uptake were determined with VR1eGFP-transfected cells (*open circles*). *b,* demonstration of vanilloid binding activity of the VR1eGFP (*squares*) and VR1ϵ (*diamonds*) chimeric constructs expressed in COS7 cells. [^{3}H]RTX binding experiments were carried out 48 h following the transfection as described under "Experimental Procedures." The results were analyzed by fitting the Hill equation to the data points. The effect of 10 μM CPZ on the binding of 0.5 nM [^{3}H]RTX is indicated by the *filled diamond* (VR1ϵ) and the *filled square* (VR1eGFP), respectively. Background binding was determined in cells transfected with a control plasmid (eGFP, *filled circles*). Results are from a single experiment carried out with triplicate determinations. Two additional experiments yielded similar results.

detected in cells transfected with the plasmid expressing only eGFP (Fig. 3*b*).

Confocal fluorescence microscopy was employed to analyze the intracellular distribution of VR1eGFP. Optical sections taken at the plane of cell attachment to the glass surface show VR1eGFP fluorescence in the plasma membrane, where microvilli were labeled (Fig. 4*a*, VR1 accumulation also is present at the focal points in this plane, not seen with fluorescent markers of ER). Optical sections taken through the middle of the cell nucleus, disclosed VR1eGFP in intracellular structures consistent with the ER (Fig. 4, *b versus d*). To confirm ER localization, cells were transfected with an eGFP that was C-terminally tagged with the ER retention signal (*i.e.* the KDEL motif, Fig. 4*b*). Visualization of the transiently expressed eGFP-KDEL chimera protein in COS7 cells verified that VR1eGFP indeed stained the same ER compartment within the cytoplasm and around the nucleus (Fig. 4, *b versus d*). Furthermore, the same ER colocalization result was obtained when VR1eGFP-expressing cells were costained with the ER-tracker vital dye (Molecular Probes) (not shown). Fig. 4 illustrates localization of VR1 in COS7 cells but a similar ER localization was seen in HEK293 and NIH 3T3 cells, indicating that it is not a cell type-specific anomaly. ER localization was observed over a range of transfection efficiencies, and the distribution between the plasma membrane and ER was similar in cells expressing VR1eGFP at different levels (not shown). The proportionality between plasma membrane and ER also was maintained in a cell line stably expressing relatively lower levels of VR1ϵ from the noninduced MTH promoter. These data, as well as results from immunocytochemical staining of fixed DRG neurons, which show a high density of staining throughout the neuronal cytoplasm (10), suggest the distribution is not simply due to overexpression. Dual wavelength imaging studies demonstrated that the intracellular compartment containing VR1eGFP (*green*) was distinct from the filamentous mitochondria (*red*), which were labeled by the red MitoTracker dye and are generally much thicker than the ER (Fig. 4*f*).

Previously it was noted that addition of ionomycin to cells induces intracellular membrane fragmentation due to permeabilization of the plasma membrane to cations (22). This was verified in baseline control studies using the eGFP-KDEL-expressing plasmid, which showed that ionomycin treatment induced membrane fragmentation of the ER (Fig. 4, *b versus c*). This fragmentation was identical to what occurred with VR1eGFP-expressing cells upon exposure to 1 nM RTX. In these cells a 20-s exposure induced fragmentation of the ER (Fig. 4, *d* and *e*) and, simultaneously, a rounding up of the filamentous mitochondria (Fig. 4, *f versus* g). Testing of a second vanilloid ligand, CAP (1 μM), also demonstrated membrane fragmentation with similar dynamics as noted with RTX (not shown). With the appropriate sets of fluorescence filters, we observed no mixing between the VR1eGFP vesicles (*green*) and the mitochondrial membranes (*red*) (data not shown). In cells expressing only eGFP, the structure of the mitochondria and ER did not change upon exposure to vanilloids, indicating the dependence for these effects on the presence of the VR1 receptor. Thus, within the first few seconds after vanilloid exposure, coincident and structurally similar intracellular organelle remodeling occurs for both the ER and the mitochondria.

The effect of RTX on cytosolic Ca^{2+} was studied by microfluorometry in transfected cells loaded with the Ca^{2+}-monitoring dye, Fura-2 AM. The resting $[Ca^{2+}]_i$ was similar (~50 nM) in COS7 cells transfected with either VR1eGFP or eGFP plasmids. Addition of 1 nM RTX induced a rapid (within 10 s) elevation of $[Ca^{2+}]_i$ in VR1eGFP-expressing cells which peaked at 500 nM at ~1 min ($n = 3$) and, consistent with the concurrent ER and mitochondrial damage (Fig. 4, *e* and *g*), did not return to resting levels (Fig. 5*a*). In the absence of external Ca^{2+}, the RTX-induced increase in $[Ca^{2+}]_i$ was temporally delayed from ≤10 s to ~1 min (see Figs. 7 and 8). No increase in $[Ca^{2+}]_i$ was observed in cells expressing only eGFP ($n = 3$) (not shown).

The preceding experiments focused on events occurring within the first few seconds following exposure to VR1 agonists. To extend the time of cellular observation, serial 1-s confocal microscopy scans were performed at 1-min intervals on live VR1eGFP-expressing cells. In these experiments the early events occurred as described (*e.g.* transmembrane Ca^{2+} flux, intracellular remodeling, within 30 s in 13 out of 15 cells). Within 3 min after RTX administration, the nuclear membrane was outlined with VR1eGFP fluorescence, and ER membrane vesicles were observed around the nucleus (Fig. 5*c*). Then, progressively growing blebs were noted in the nuclear membrane (2 out of 10 at 5 min and 9 out of 10 cells at 10 min). In the cell shown, the membrane degradation concluded with bursting of the plasma membrane at 43 min (Fig. 5*c*). Other

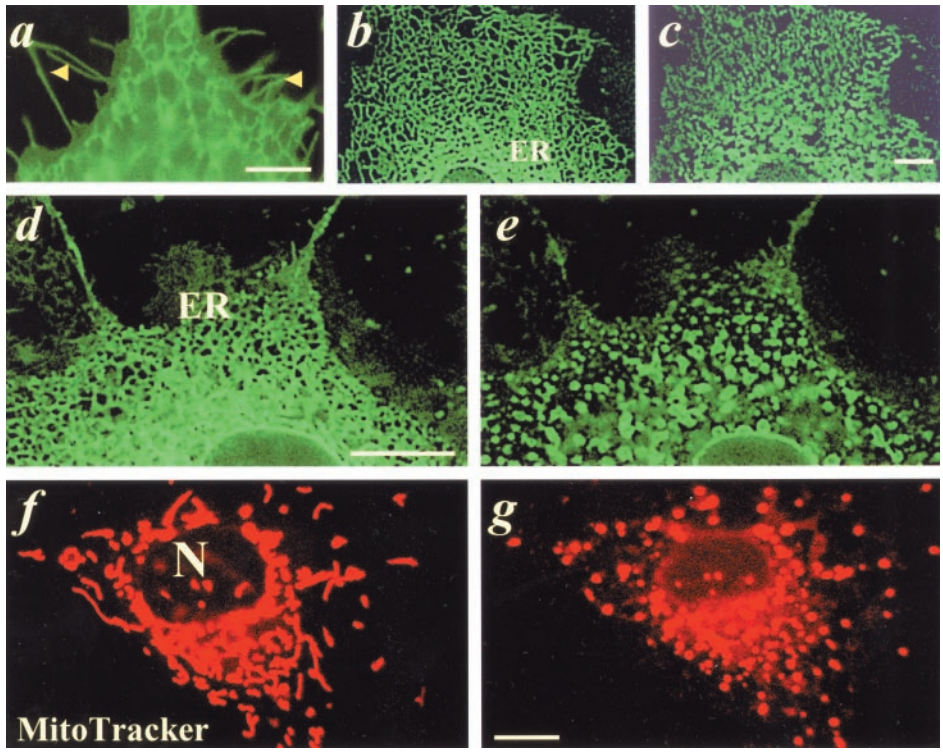

FIG. 4. **Early dynamics of VR1 activation imaged in live cells.** To determine the *in vivo* cellular location of the fluorescently labeled VR1eGFP (*a*, *d,* and *e*), studies with eGFP-KDEL (*b* and *c*) and MitoTracker vital dyes (*f* and *g*) were carried out 24 h after transfection in COS7 cells employing laser confocal microscopy. In optical sections close to the glass surface VR1eGFP was localized in microvilli at the plasma membrane in transiently transfected live COS7 cells (*a*). The bright spots are the focal points at the basal membrane glass interface. *Arrowheads* show the extrusion of VR1eGFP-labeled plasma membrane microspikes at the edge of the cell. In median optical sections, at level of the cell nucleus, VR1eGFPs are depicted in an intracellular membrane network similar to ER (*d*). Similarities in eGFP-KDEL and VR1eGFP in this optical section verify that VR1 indeed can localize to the ER compartment. To study the effects of ionomycin (4-bromo-A23187) on intracellular membranes, the same cell was imaged by the expressed ER marker, eGFP-KDEL (*b* and *c*) before and 10 s after addition of 4 μM ionophore. The effects of RTX treatment were depicted with the VR1eGFP (*d* and *e*) and MitoTracker (*f* and *g*)-derived fluorescence before and 20 s after addition of 1 nM RTX. The membrane permeabilization to cation by ionomycin or activation of VR1 by RTX resulted in a similar ER vesiculation (*c* and *e*), indicative of similar mechanism and vesiculation of the mitochondria (*g*). *Bar,* 5 μm.

cells displayed similar nuclear changes and cell disruption within 1–2 h (3 out of 5 within 1 h and 5 out of 5 monitored for 2 h in one experiment). Lower doses of RTX (≤0.1 nM) evoked slower nuclear membrane fragmentation but eventually resulted in cell lysis (4 out of 4 cells within 3 h). The effects were not due to the repetitive scanning, since single scans of transfected cells performed at 30 min after RTX administration also revealed (8 out of 8) identical effects of RTX on intracellular membrane structures.

Fig. 6 summarizes quantitatively the fluorescence scanning confocal microscopy data collected in repeated experiments. ER fragmentation was noted in 16 cells within 6 s of adding 1 nM RTX; vesiculation was completed within 1 min in each cell monitored (scans were done every 6 s, $n = 30$). ER vesiculation directly corresponded to the time course determined for RTX-induced $[Ca^{2+}]_i$ accumulation (Fig. 5*a*). The first nuclear bleb appeared 2 min after RTX treatment (2 out of 30) and then each observed cell ($n = 30$) showed at least 1 bleb by 10 min. Cell lysis started as early as 10 min after RTX addition (1 out of 30 cells) and was complete within 2 h (30 out of 30 cells).

To explore potential activity of the ER-localized VR1, COS7 cells expressing VR1eGFP were treated with 1 nM RTX in the absence of extracellular Ca^{2+}. VR1eGFP-expressing cells, prewashed extensively in 1 mM EGTA, showed vesiculation of the ER and disruption of mitochondria similar to that determined in the presence of 1 mM extracellular Ca^{2+} (Figs. 4 and 5). However, the time required for these changes was much longer, on the order of minutes rather than seconds. The first obvious signs of ER fragmentation and round up of mitochondria were noted at ~3 min after 1 nM RTX addition (5 out of 5). Nontransfected cells ($n = 2$) in the same microscopic field showed an intact mitochondrial structure as determined by MitoTracker fluorescence, indicating that the vanilloid effects on the intracellular membranes were specific to those cells expressing VR1eGFP (Fig. 7). If the extracellular Ca^{2+} concentration was adjusted back to 1 mM in the presence of 1 nM RTX, it triggered an abrupt ER fragmentation (within 1–3 s in 5 out of 5 cells) demonstrating the pivotal function of Ca^{2+} in this process (data not shown). These data suggest that the ER-localized VR1 mobilizes calcium from the ER but that $[Ca^{2+}]_i$ accumulation occurred more slowly or that the amounts were such that the $[Ca^{2+}]_i$ accumulation was buffered and more time was required to reach toxic cytoplasmic concentrations.

The quantitative aspects of calcium release from internal stores are presented in Fig. 8, which examines both DRG neurons, and transiently transfected COS7 cells. In recording medium containing zero extracellular Ca^{2+}, ratio imaging of VR1eGFP-positive COS7 cells (exhibiting medium or low green fluorescence intensity, Fig. 8*a*) or small size DRG cells (Fig. 8*b*) demonstrated dramatic increases in the 405/485 ratio after administration of RTX. Control nontransfected COS7 cells did not show any change in the 405/485 ratio when exposed to RTX. As noted above, the increase in $[Ca^{2+}]_i$ in the zero extracellular Ca^{2+} conditions was temporally delayed, requiring ~1 min. By comparison, cells exposed to RTX in the presence of 1 mM extracellular Ca^{2+} exhibit an increase within ≤10 s. The ~45–50-s delay also occurred in small size DRG neurons (Fig. 8*b*). The RTX-induced ratio increase in cells expressing VR1eGFP, and small size DRG neurons indicates Ca^{2+} release from internal stores and $[Ca^{2+}]_i$ accumulation in the cytosol. These ex-

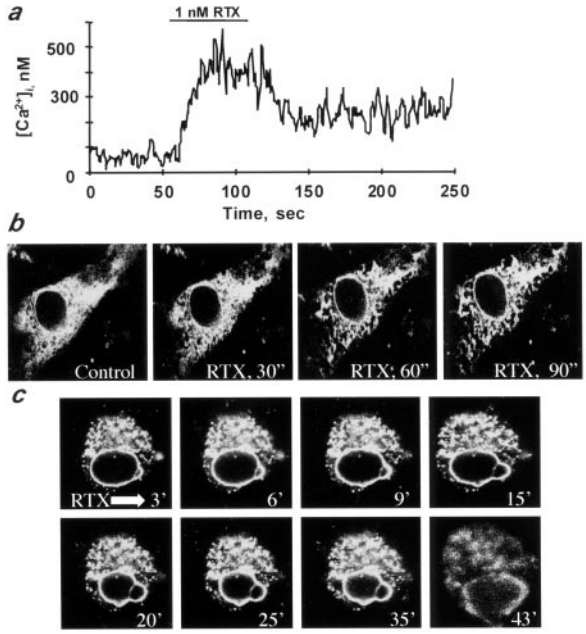

FIG. 5. **Ca^{2+} microfluorometry and cell death.** For microfluorometry of intracellular free Ca^{2+} (*a*), VR1eGFP-expressing COS7 cells were cultured and transfected in glass bottom dishes and then loaded with the Ca^{2+} indicator dye Fura2/AM for 30 min. Single VR1eGFP-transfected cells were first identified by their green fluorescence. Once the cell was in focus, microfluorometric determinations of $[Ca^{2+}]_i$ were carried out for 60 s and then 1 nM RTX was perfused for 1 min as indicated. To reduce the noise of single cell recordings 5 consecutive data points were averaged. *b,* live cell imagings of short term membrane remodeling due to RTX treatment were carried out in COS7 cells expressing VR1eGFP. RTX (1 nM) was added 24 h after transient transfection, and selected cells were scanned for 1 s at 30-s intervals as indicated. Remodeling of the ER started within 30 s, coincident with the rise in $[Ca^{2+}]_i$. *c,* for long term *in vivo* monitoring of RTX effects, cells were continuously perfused in an imaging chamber for 1 h. Following 3 min of perfusion, a representative VR1eGFP-expressing cell was selected and imaged by 1-s laser scanning at 1-min intervals for 45 min. Nuclear blebs became apparent within 3 min, and cell lysis occurred 43 min after the RTX was administered. Other cells displayed similar loss of integrity, and the data are summarized graphically in Fig. 6.

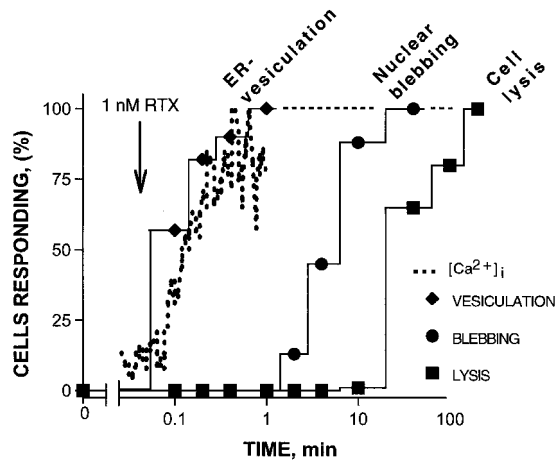

FIG. 6. **Quantitative analysis of membrane changes due to 1 nM RTX treatment depicted by confocal microscopy.** Imaging data were derived from 30 independent transient transfection experiments carried out with VR1eGFP-expressing COS7 cells; cells exhibiting an intermediate level of fluorescence were chosen for imaging. *Symbols* at each step of the three graphs represent the percentage of cells from the 30 cells imaged responding within the time frames indicated (*e.g.* the *1st diamond* indicates that 16 cells responded with ER vesiculation within 1–6 s). The *dotted line* superimposed on the graphs represents the smoothed accumulation curve of $[Ca^{2+}]_i$ from Fig. 5. The entire tubular ER network, decorated with VR1eGFP previous to 1 nM RTX treatment, changed into circular ER vesicles (*diamonds*); the first nuclear blebs were observed at ~2 min (*circles*). Loss of cell membrane integrity was seen in 1 cell out of 30 at 10 min and progressed until lysis of all 30 cells was complete at ~2 h (*squares*).

periments suggest that the intracellular VR1 is functional and that RTX, a lipid-soluble agonist of VR1, can indeed act as an agonist at these intracellular sites.

To verify that the rapid intracellular membrane changes observed in heterologous cells expressing VR1 also occurred in small-size DRG neurons, experiments were carried out on primary cultures from DRG (Fig. 9). Cultures were preincubated with the MitoTracker dye and then exposed to 1 nM RTX. Small size neurons were selected and monitored by confocal microscopy employing 1-s scans every 20 s before and after treatment with vanilloids. Neurons in this size range were previously determined to be VR1-positive with an antibody raised against the N-terminal 18 amino acids of VR1 (data not shown). The MitoTracker dye revealed normal, slightly elongated mitochondria in untreated small size DRG neurons (Fig. 9*a*). Treatment with RTX induced the mitochondria to fragment within 20 s (Fig. 9*b*), similar to the kinetics observed in COS7 cells ectopically expressing VR1eGFP (Fig. 4, *d versus e*). RTX at 1 nM concentration was without effect on mitochondria localized in the glial cell population (Fig. 9*c*) or in nearby large neurons within the field of view (data not shown).

The above experiments demonstrated that vanilloids rapidly target the ER and mitochondria at the cell body in small size DRG neurons expressing VR1, producing effects within seconds. To address the effects on DRG neurons of longer exposure to RTX, DRG cultures were subjected to dual wavelength fluorescent imaging. Cultures were loaded with Indo-1 AM and then incubated in HBSSH containing 1 mM $CaCl_2$. Propidium iodide (PI) was added to the imaging chamber just before the cultures were examined with confocal microscopy. In repeated experiments, specific neurons in the field of view demonstrated instant increases in $[Ca^{2+}]_i$ (within seconds) upon administration of 25 nM RTX. Neurons exhibiting the RTX-induced increase in $[Ca^{2+}]_i$ started to accumulate PI in the nucleus ~40 min after addition of RTX; a time that coincides with loss of plasma membrane integrity in VR1eGFP-expressing COS7 cells exposed to RTX (Figs. 5 and 6). In the same microscopic field there were neurons that neither responded to RTX with an elevation in $[Ca^{2+}]_i$ nor accumulated PI even after 2 h of exposure (Fig. 10). This result is consistent with the idea that these neurons do not express VR1 and reinforces the cellular and molecular specificity of vanilloid actions on DRG neurons. Repeated time course observations with DRG cultures indicated similar dynamics for DRG neuronal death as described for transiently (see Fig. 6) or stably transfected NIH 3T3 cells (not shown) expressing recombinant VR1.

Elevated $[Ca^{2+}]_i$ can induce cytotoxicity within minutes to hours in VR1-expressing cells or specific DRG neurons, as demonstrated in previous experiments. This suggests that vanilloid application to the perikarya may be an effective means for specific deletion of nociceptive neurons. To study this phenomenon, 1-week-old DRG cultures from rats were treated with 50 μM olvanil (OLV, a long chain fatty acid modified synthetic vanilloid) or 25 nM RTX for 48 h. From these cultures, total protein extracts were prepared in denaturing SDS sample buffer (Fig. 11). Western blot of VR1 protein and densitometry of films after enhanced chemiluminescence visualization revealed that olvanil treatment almost completely eliminated (99% decrease) neurons expressing VR1 from the culture. RTX, employed at a concentration 2,000-fold less than OLV, eliminated ~80% of the neurons expressing VR1. Other cell types present in the DRG culture were not affected after 48 h of

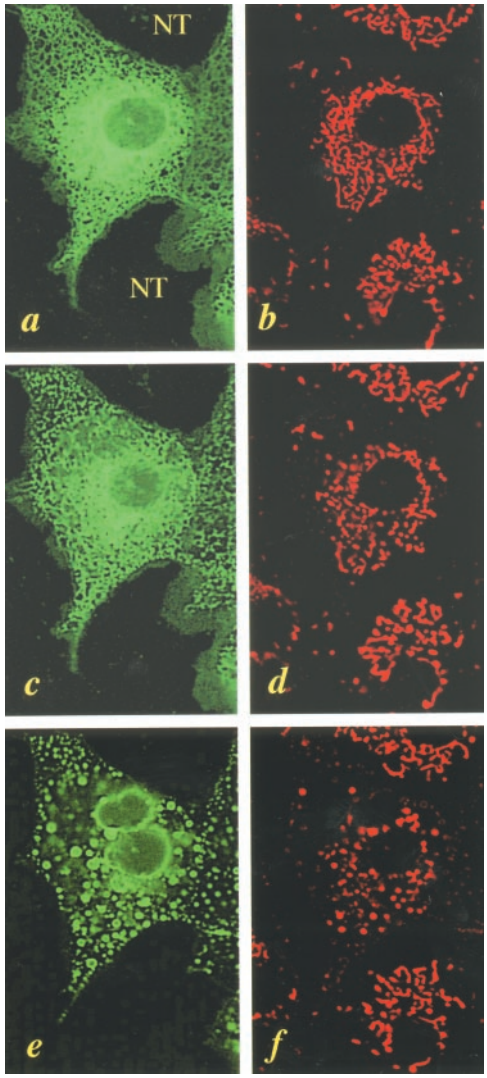

FIG. 7. **Live COS7 cells expressing VR1eGFP are depicted after extensive washing in 1 mM EGTA and incubation in calcium-free media.** *a, NT* stands for nontransfected cells that cannot be seen in *a* but visualized by the red fluorescent MitoTracker dye *b*. The cells from the same microscopic field were then treated with 1 nM RTX in the absence of Ca^{2+} and monitored with the green and red channels. The slow laser scanning (3 times for 1 s) and Kalman filtering option of the confocal microscope were employed in each minute to take pictures on both channels. At 3 min, pronounced reorganization of the ER and mitochondrial membranes was noted (*c* and *d*), which progressed to fragmentation of the ER and rounding up of the mitochondria at 10 min (*e* and *f*) in VR1eGFP-expressing cells. Mitochondria in nontransfected cells did not show these intracellular changes due to RTX treatment (*b versus d* and *f*). For the repeated time series, cells were stained with 250 nM MitoTracker dye 30 min before confocal microscopy. VR1eGFP-transfected cells were selected randomly and monitored up to 30 min after the RTX addition. Similar results were obtained in three additional independent experiments.

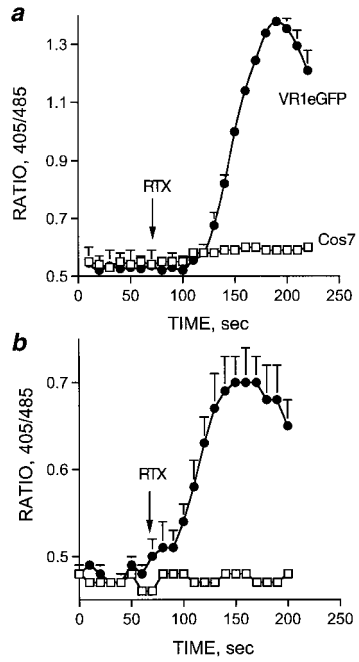

FIG. 8. **RTX-induced mobilization of Ca^{2+} from internal sources in the absence of extracellular Ca^{2+}.** DRG and VR1eGFP-expressing cultures were prepared as described under "Experimental Procedures." For ratiometric confocal imaging, DRG neurons and VR1eGFP-expressing cells were pre-loaded with 5 μM Indo-1 AM dye. After incubation for 30 min at 34 °C the cells were washed three times in HBSSH containing 1 mM EGTA to remove extracellular Ca^{2+} and excess dye. Group of transiently transfected cells expressing VR1eGFP (*a*) and primary cultures of DRG neurons (*b*) were selected and then perikarya marked for ratiometric imaging in the field of a 40 × objective. RTX was added to make a 1 nM final concentration in the medium. The ratio of emitted fluorescence intensity at 405 and 485 was calculated from images taken at 10-s intervals. *a,* data shown are from a field of view containing three VR1eGFP-transfected and three nontransfected COS7 cells. *b,* primary sensory neuronal showed similar mobilization of Ca^{2+} from intracellular stores. The graph is from three neurons exhibiting a Ca^{2+} response and two neurons that did not show a change in fluorescence ratio. Data were replicated in three other cultures, which also showed Ca^{2+} mobilization from intracellular sources, as illustrated here.

treatment with OLV or RTX, as assessed by re-probing the same Western blots with an antibody recognizing the common tissue protein cytochrome *c* (Fig. 11).

DISCUSSION

The present paper investigates the early cellular dynamics of vanilloid-triggered events through *in vivo* expression of fluorescent- and epitope-tagged recombinants of rat VR1. Extension of the C terminus with the 27-kDa eGFP did not compromise the electrophysiological function of VR1 upon expression in heterologous cell systems and tagging with either eGFP or a short 12-amino acid ϵ-epitope did not affect vanilloid-induced ionophore function as assessed by $^{45}Ca^{2+}$ uptake. The ultrapotent vanilloid, RTX, binds with nanomolar affinity to both VR1eGFP and VR1ϵ. The binding and $^{45}Ca^{2+}$ uptake parameters are similar to those reported either for the nonchimeric VR1 or for rat DRG primary cultures (3, 4, 14, 23–26). The electrophysiology of VR1eGFP-expressing cells showed that vanilloids rapidly induced an inward current flow that was blocked by CPZ, as described for wild-type VR1 (9). Vanilloid-induced $^{45}Ca^{2+}$ uptake and [^{3}H]RTX binding were also inhibited by CPZ, further supporting the specific interaction of vanilloids with the tagged VR1 variants. VR1eGFP and VR1ϵ mimic the wild-type receptor and are thus useful reporters with which to study the dynamics of VR1 activation by vanilloids, other modulators, and physical stimuli.

In addition to localization at the plasma membrane, VR1eGFP was demonstrated in the ER by colocalization with the fluorescent ER-tracker dye in live COS7, HEK293, and NIH 3T3 cells, as determined using high resolution confocal microscopy. One of the benefits of this localization and fluorescent tagging was the elucidation of the abrupt ER fragmentation due to agonist treatment. Addition of RTX to VR1-expressing cells induced ~10-fold accumulation of $[Ca^{2+}]_i$. This coincided with the rapid transformation of the normal lattice-like ER membrane structure into rounded vesicles, the earliest hallmark of Ca^{2+} cytotoxicity observed in living cells so far

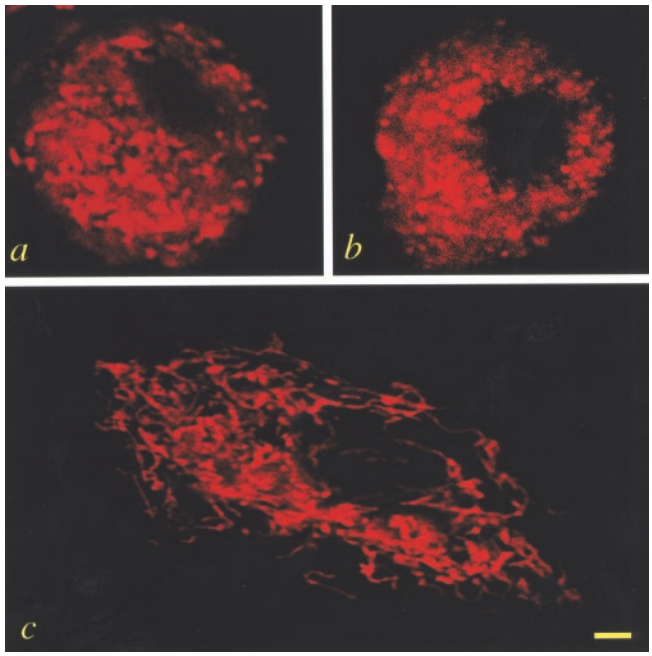

FIG. 9. **Live confocal imaging of MitoTracker dye stained, small size DRG neurons.** Cultures were prepared from E16 rats and maintained on 25-mm laminin-coated glass coverslips in DMEM containing NGF and FUDR for 1 week before confocal microscopy as described under "Experimental Procedures." After incubation for 30 min in 250 nM MitoTracker dye, cells were washed two times and examined in HBSSH containing 1 mM Ca^{2+} (*a*) and then RTX was added to make a 1 nM final concentration. Cells are depicted 20 s after the treatment (*b*). Mitochondria of a glial cell are shown from the same culture 10 min after the RTX treatment (*c*). In the spherical neuronal perikarya, the otherwise elongated mitochondria are packed densely (*a*), but the fragmentation due to RTX is evident (*b*), especially when compared with well preserved mitochondria, depicted in the large, flat glial cell from the same culture after vanilloid drug administration (*c*). The glial cell shown is typical; none of the glia in the culture were affected by RTX. *Scale bar,* 2 μm.

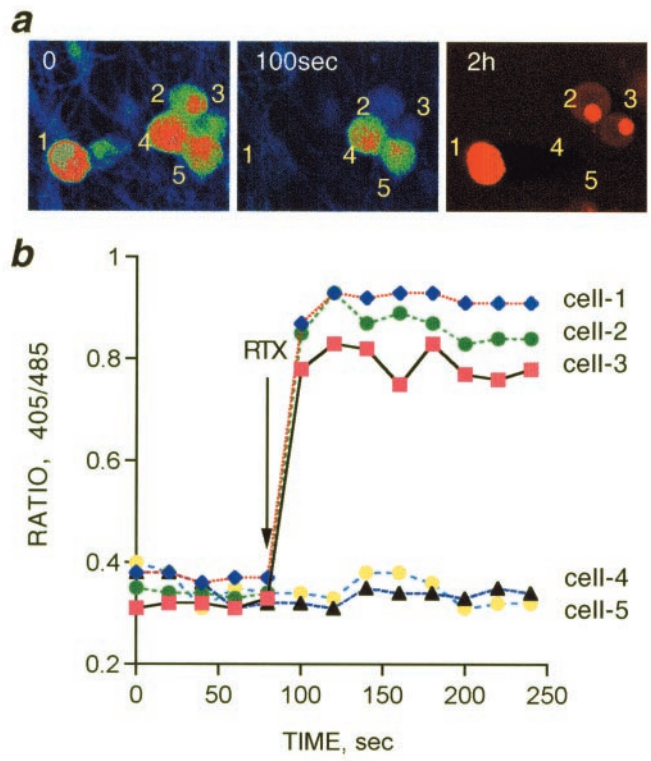

FIG. 10. **Relationship between RTX-induced accumulation of $[Ca^{2+}]_i$ and cell death in DRG neurons.** Cells were examined by confocal microscopy at 405 and 485 nm. Individual cells are numbered in *a* and ratios of 405/485 of the numbered neurons are plotted in *b*. Dissociated DRG neurons were seeded on poly-D-lysine pre-coated coverslips. Cultures were loaded with the Indo-1 AM, 30 min before the experiments, and then washed and changed into recording medium containing 1 mM $CaCl_2$. PI was added just before confocal microscopy (40 × objective). First, ratio imaging at 405 and 485 nm was carried out. Frames taken on the 485 nm channel are shown, employing a geographic look-up table (*a*, 0 and 100 s). PI fluorescence was depicted on the red channel at 2 h, as indicated. RTX (25 μM), added at 70 s, induced an instant change in the 405/485 ratio as illustrated visually by the denominator channel (*a*, 0 and 100 s), and plotted in *b*. In some neurons (*cell-1, -2,* and *-3*) the *red* color shifted in the *blue* direction, indicative of a steep elevation in $[Ca^{2+}]_i$ (within seconds). In other cells (*cell-4* and *-5*) little change in color (*red*) indicated a steady, low basal level of $[Ca^{2+}]_i$. The identical cells that reacted to RTX with an elevated $[Ca^{2+}]_i$ also accumulated PI in the nucleus (*cell-1, -2,* and *-3*), indicating plasma membrane damage (*a*). Neurons resistant to RTX-induced elevation of $[Ca^{2+}]_i$ excluded PI even after 2 h (*cell-4* and *-5*). Similar results were recorded in two additional DRG cultures.

(Fig. 6). Calcium-induced ER vesiculation occurred throughout the cytoplasm (*i.e.* the *z*-stack of confocal acquisition), similar to that described previously for ionomycin (22). This type of membrane rearrangement (Figs. 4, 5, and 7) is clearly distinct from the agonist-mediated endocytosis, which can occur with nonion channel transmembrane receptors. In addition to the ER, the live cell imaging experiments revealed other membrane compartments that reacted to the vanilloid-induced elevated $[Ca^{2+}]_i$. These include the following: (i) shedding of the plasma membrane; (ii) intracellular fragmentation of mitochondria; and later (iii) blebbing of the nuclear envelope; (iv) accumulation of propidium iodide in the cell nucleus; and (v) rupture of the plasma membrane (Figs. 4, 5, 9, and 10).

The intracellular location of VR1 was separable from the mitochondrial compartment as assessed concurrently with the red MitoTracker dye (Figs. 4 and 7). Although spatially distinct, both the ER and mitochondria fragmented in seconds upon the large increase in $[Ca^{2+}]_i$ through VR1 (Figs. 4, 5, 9, and 10). The staining of the mitochondrial compartment with the MitoTracker vital dye provided a surrogate end point to extend our findings in transiently transfected cells to DRG neurons in primary culture where specific small sized neurons showed the same immediate early changes in mitochondrial structure when exposed to vanilloids (Figs. 4, 7 *versus* 9). However, the perikarya of the responding neurons are spheroid rather than flat and extended, and a much smaller volume is available for confocal microscopy due to the high nucleus/cytosol ratio. Thus, in contrast to the flattened COS7 cells, geometry and size make nociceptive neurons less favorable subjects for live cell imaging of elongated organelles such as the mitochondria and the ER. As expected for the restricted cellular expression of VR1 in the DRG (9), RTX did not affect the mitochondria of adjacent large neurons or glia, imaged at the same time (Fig. 9).

The potential role of ER-localized VR1 is not yet clear, and we continue to investigate it. Our studies in calcium-free media show that a similar vanilloid-induced, VR1-specific remodeling of ER can occur with Ca^{2+} mobilized from intracellular sources, although with a much slower time course. Orientation or folding of VR1 in the ER may be factors, but the lag period in heterologous systems and DRG neurons (Figs. 7 and 8) also suggests buffering mechanisms are present (*i.e.* mitochondrial Ca^{2+} uptake (27)) or that multiple steps are required for activation of ER-localized ion channels (22, 28). The delay is not due to lack of membrane penetration of vanilloids, which are highly lipid-soluble. In fact, the water-soluble CAP analogue DA-5018 can only bind to VR1 when applied intracellularly, implying that vanilloids first must traverse the plasma membrane for activation of VR1 Ca^{2+} signaling (29). Other investi-

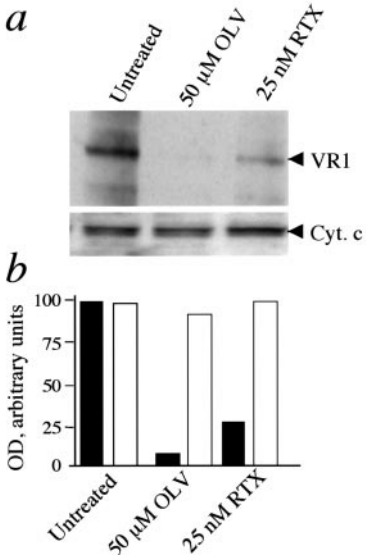

FIG. 11. **Effect of long term vanilloid treatments on rat DRG cultures.** Dissociated DRG cells from E16 rats were seeded in 24-well plates and cultured for 1 week in the presence of NGF and FUDR, as described under "Experimental Procedures." Cells were then treated with 50 μM OLV or 25 nM RTX for 48 h. Total cell extracts were prepared from each well by sonicating the samples in SDS sample buffer for 10 s; and then 25 μg of proteins were separated in an SDS gradient gel (4–20%) for Western blotting. VR1-specific immunoreactivity was determined with an antibody raised and immunopurified against the N-terminal 18 amino acids of rat VR1. An enhanced chemiluminescent method was employed to visualize the VR1-specific immunocomplex (*a*). To show that the treatment with vanilloids affected only the VR1-expressing cells, the filter was stripped of the VR1-specific primary antibody and re-probed with an antiserum specific to cytochrome *c* (*Cyt. c*), as indicated. X-ray films were scanned, and bands were analyzed for optical density by the NIH Image (version 1.61) software. *b, bar graph* shows optical densities from a representative experiment obtained from the same batch of DRG cultures. Similar results were obtained from a second independent repetition of the experiment.

gations (30–32) have shown that removal of extracellular calcium diminishes but does not eliminate physiological effects in a variety of systems including vanilloid-evoked inward currents with repeated administration of vanilloids in cultured DRG neurons. Furthermore, it was observed that capsaicin stimulated release of substance P from C-fibers in the absence of extracellular Ca^{2+} (33). Here we positively identified a delayed but RTX-induced Ca^{2+} release from intracellular stores in zero extracellular Ca^{2+}, implying an important role of ER-localized VR1 (Fig. 8). These observations, together with previous electrophysiological data (30, 31), indicate that, in addition to the plasma membrane exposed VR1, a novel, functional, intracellular (*i.e.* ER) pool exists in DRG neurons. The results are consistent with the interpretation that, in the ER, VR1 gates Ca^{2+} stores which respond to vanilloids by releasing Ca^{2+} to the cytosol (Figs. 7–10).

Our data show that, as time progresses, the vanilloid-induced elevation in cytosolic Ca^{2+} produces an evolving cytotoxicity. Within 10 min, progressive nuclear blebbing is seen which coincides with PI incorporation in the nucleus, followed by lysis of the plasma membrane and cell death in 1–2 h in both VR1-expressing cells and DRG neurons. These more long term events are shown as a series of single frames in Figs. 5 and 10; however, upon replay of the frames from transfected cells or DRG neurons as a video clip (not shown), the vanilloid-induced PI accumulation in the cell nucleus and cell lysis highlights the dramatic nature of the cell death. The selectivity is also apparent since adjacent nontransfected or non-VR1-expressing cells remain resistant to PI permeation (Fig. 10).

Double wavelength imaging of consecutive accumulation of $[Ca^{2+}]_i$ and propidium iodide due to RTX treatment and Western blot analysis of VR1 in primary DRG cultures all support the selectivity of vanilloid-induced cell deletion. Western blot data from DRG cultures (Fig. 11), together with images of cells heterologously expressing VR1eGFP (Fig. 5) or of DRG neurons (Fig. 10), indicate that RTX treatment first compromises the function of cell organelles and then kills the cell. These data argue against specific VR1 proteolysis or desensitization of VR1 by limited endo- or exocytosis as mechanisms mediating VR1 protein elimination from the primary cultures.

Several mechanisms can govern the intracellular remodeling and cell death that occur upon exposure to vanilloids. The most likely is rapid Ca^{2+} toxicity following VR1 activation, which is consistent with the data presented here from VR1-expressing cells and DRG neurons (Figs. 4–11) and by others (9, 27). Although the primary steps of Ca^{2+} toxicity are similar to apoptosis, including nuclear blebbing and PI staining of the nucleus (34), chromatin fragmentation, apoptotic body formation, and caspase activation were not apparent within 24 h (data not shown). Previous studies characterized only the terminal phase of vanilloid-induced cellular changes in detail. The longer term dynamics visualized with VR1eGFP in the present study are consistent with those noted with end point observations in the DRG, including intracellular membrane fragmentation, mitochondrial swelling, and nuclear envelope segmentation (8, 34–36). By extension, these results are generalized to a variety of ligand-operated Ca^{2+} channels such as the excitatory amino acid *N*-methyl-D-aspartic acid receptor, which can be activated by potent toxic ligands (37, 38).

The present data suggest a new potential therapeutic use of vanilloids, which is the targeted removal of nociceptive primary afferent neurons. Among the wide variety of VR1 agonists, OLV may have several advantages for clinical application. It is reported not to cause painful activation of the nociceptive afferent ending and, therefore, may be less inflammatory than other vanilloids (39). Our data also show that OLV is nontoxic to cells devoid of VR1 up to 50 μM, yet this concentration almost completely and specifically removes VR1-expressing cells in DRG culture (Fig. 11). Clinical application of vanilloids could be made regionally selective by the use of image-guided intraganglionic or nerve root administration to trigger specifically increases in $[Ca^{2+}]_i$ at the level of the neuronal perikarya in sensory ganglia involved in a pathological pain state. Preclinical data based on our experience with epidural RTX or capsaicin administered to adult rats (5, 40) suggest that loss of C fibers via this approach would be an effective means for pain control.

In summary, our data refine the early dynamics of Ca^{2+} cytotoxicity in VR1-expressing cells. Fluorescent imaging in live cells revealed that at least three vital organelles are immediately damaged due to increased $[Ca^{2+}]_i$ conferred by the agonist-activated VR1. One is the ER, which reacts with abrupt fragmentation. The others are the mitochondria and cell nucleus. These organelles are present in the cell body of sensory neurons; therefore, disruption of their function equally can contribute to desensitization and elimination of VR1-expressing cells (5). Our primary culture experiments suggest that precise targeting of vanilloids to the perikarya in sensory ganglia can induce specific elimination of VR1-positive cells by Ca^{2+} cytotoxicity, characterized here in detail. A similar strategy may have clinical utility in select conditions to remove nociceptive neurons causing intractable pain in humans.

REFERENCES

1. Hylden, J. L., Noguchi, K., and Ruda, M. A. (1992) *J. Neurosci.* **12,** 1716–1725
2. Jancso, G., Kiraly, E., and Jancso-Gabor, A. (1977) *Nature* **270,** 741–743
3. Szallasi, A., Nilsson, S., Farkas-Szallasi, T., Blumberg, P. M., Hokfelt, T., and

Lundberg, J. M. (1995) *Brain Res.* **703,** 175–183
4. Farkas-Szallasi, T., Bennett, G. J., Blumberg, P. M., Hokfelt, T., Lundberg, J. M., and Szallasi, A. (1996) *Brain Res.* **719,** 213–218
5. Szabo, T., Olah, Z., Iadarola, M. J., and Blumberg, P. M. (1999) *Brain Res.* **840,** 92–98
6. Yaksh, T. L., Farb, D. H., Leeman, S. E., and Jessell, T. M. (1979) *Science* **206,** 481–483
7. Winter, J., Dray, A., Wood, J. N., Yeats, J. C., and Bevan, S. (1990) *Brain Res.* **520,** 131–140
8. Jancso, G., and Lawson, S. N. (1990) *Neuroscience* **39,** 501–511
9. Caterina, M. J., Schumacher, M. A., Tominaga, M., Rosen, T. A., Levine, J. D., and Julius, D. (1997) *Nature* **389,** 816–824
10. Tominaga, M., Caterina, M. J., Malmberg, A. B., Rosen, T. A., Gilbert, H., Skinner, K., Raumann, B. E., Basbaum, A. I., and Julius, D. (1998) *Neuron* **21,** 531–543
11. Davis, J. B., Gray, J., Gunthorpe, M. J., Hatcher, J. P., Davey, P. T., Overend, P., Harries, M. H., Latcham, J., Clapham, C., Atkinson, K., Hughes, S. A., Rance, K., Grau, E., Harper, A. J., Pugh, P. L., Rogers, D. C., Bingham, S., Randall, A., and Sheardown, S. A. (2000) *Nature* **405,** 183–187
12. Caterina, M. J., Leffler, A., Malmberg, A. B., Martin, W. J., Trafton, J., Petersen-Zeitz, K. R., Koltzenburg, M., Basbaum, A. I., and Julius, D. (2000) *Science* **288,** 306–313
13. Guo, A., Vulchanova, L., Wang, J., Li, X., and Elde, R. (1999) *Eur. J. Neurosci.* **11,** 946–958
14. Szallasi, A., Blumberg, P. M., Annicelli, L. L., Krause, J. E., and Cortright, D. N. (1999) *Mol. Pharmacol.* **56,** 581–587
15. Jancso, G., Karcsu, S., Kiraly, E., Szebeni, A., Toth, L., Bacsy, E., Joo, F., and Parducz, A. (1984) *Brain Res.* **295,** 211–216
16. Kiraly, E., Jancso, G., and Hajos, M. (1991) *Brain Res.* **540,** 279–282
17. Olah, Z., Lehel, C., Jakab, G., and Anderson, W. B. (1994) *Anal. Biochem.* **221,** 94–102
18. Acs, G., Lee, J., Marquez, V. E., and Blumberg, P. M. (1996) *Brain Res. Mol. Brain Res.* **35,** 173–182
19. Endrenyi, L., Fajszi, C., and Kwong, F. H. (1975) *Eur. J. Biochem.* **51,** 317–328
20. Hough, C. J., Irwin, R. P., Gao, X. M., Rogawski, M. A., and Chuang, D. M. (1996) *J. Pharmacol. Exp. Ther.* **276,** 143–149
21. Grynkiewicz, G., Poenie, M., and Tsien, R. Y. (1985) *J. Biol. Chem.* **260,** 3440–3450
22. Subramanian, K., and Meyer, T. (1997) *Cell* **89,** 963–971
23. Acs, G., Biro, T., Acs, P., Modarres, S., and Blumberg, P. M. (1997) *J. Neurosci.* **17,** 5622–5628
24. Biro, T., Brodie, C., Modarres, S., Lewin, N. E., Acs, P., and Blumberg, P. M. (1998) *Brain Res. Mol. Brain Res.* **56,** 89–98
25. Biro, T., Maurer, M., Modarres, S., Lewin, N. E., Brodie, C., Acs, G., Acs, P., Paus, R., and Blumberg, P. M. (1998) *Blood* **91,** 1332–1340
26. Szallasi, A., Jonassohn, M., Acs, G., Biro, T., Acs, P., Blumberg, P. M., and Sterner, O. (1996) *Br. J. Pharmacol.* **119,** 283–290
27. Simpson, P. B., and Russell, J. T. (1998) *Brain Res. Brain Res. Rev.* **26,** 72–81
28. Berridge, M. J. (1998) *Neuron* **21,** 13–26
29. Jung, J., Hwang, S. W., Kwak, J., Lee, S. Y., Kang, C. J., Kim, W. B., Kim, D., and Oh, U. (1999) *J. Neurosci.* **19,** 529–538
30. Santicioli, P., Patacchini, R., Maggi, C. A., and Meli, A. (1987) *Neurosci. Lett.* **80,** 167–172
31. Liu, L., and Simon, S. A. (1998) *Brain Res.* **809,** 246–252
32. Usachev, Y. M., and Thayer, S. A. (1999) *BioEssays* **21,** 743–750
33. Purkiss, J., Welch, M., Doward, S., and Foster, K. (2000) *Biochem. Pharmacol.* **59,** 1403–1406
34. Earnshaw, W. C. (1995) *Curr. Opin. Cell Biol.* **7,** 337–343
35. Chiba, T., Masuko, S., and Kawano, H. (1986) *Neurosci. Lett.* **64,** 311–316
36. Sugimoto, T., Takeyama, A., Xiao, C., Takano-Yamamoto, T., and Ichikawa, H. (1999) *Brain Res.* **818,** 147–152
37. Choi, D. W. (1988) *Trends Neurosci.* **11,** 465–469
38. Yu, S. P., Yeh, C., Strasser, U., Tian, M., and Choi, D. W. (1999) *Science* **284,** 336–339
39. Dickenson, A., Hughes, C., Rueff, A., and Dray, A. (1990) *Pain* **43,** 353–362
40. Eimerl, D., and Papir-Kricheli, D. (1987) *Exp. Neurol.* **97,** 169–178